A Model for Hydrometeor Growth and Evolution of Raindrop Size Spectra in Cumulus Cells

MAN KONG YAU[1] AND PAULINE M. AUSTIN

Department of Meteorology, Massachusetts Institute of Technology, Cambridge 02139

(Manuscript received 22 March 1978, in final form 3 January 1979)

ABSTRACT

A relatively simple model of warm and cold rain microphysics in cumulus cells is developed. The proposed model avoids the large amounts of computation required in a non-parameterized treatment and yet removes some of the restrictions imposed by Kessler's microphysical parameterization. The growth of cloud droplets is bypassed, but evolution of particle size spectra for larger hydrometeors and the effects of differential fallspeeds are allowed by the growth of rain and graupel particles in a total of 25 size categories. The processes included are condensation, evaporation, accretion, collection, breakup, freezing, deposition, riming and melting. Experiments in the context of a kinematic updraft indicate results comparable to those of a stochastic model in warm rain development. It is found that a counterbalancing mechanism between autoconversion and accretion causes the results to be relatively insensitive to assumptions about the autoconversion process. Further sensitivity tests point out the important contributions of rain-rain interactions in the evolution of drop-size spectra, the essential role of impaction breakup as a limiting mechanism for drop growth, and the modes in which the presence of graupel affects the particle-size distributions.

1. Introduction

The initiation and growth of cloud and precipitation in a convective element entail physical processes of extreme complexity. A complete analysis would include consideration of the activation of cloud condensation nuclei (Fitzgerald, 1973), diffusional growth by condensation, stochastic collision and coalescence of water drops (Berry, 1967; Berry and Reinhardt, 1974a; Leighton and Rogers, 1974), drop breakup (Srivastava, 1971; Brazier-Smith *et al.*, 1973; List and Gillespie, 1976), ice particle nucleation, growth of ice crystals by deposition and aggregation, as well as stochastic collection in the growth of graupel and hail (Young, 1974a, 1974b; Cotton, 1972; Danielsen *et al.*, 1972; Scott and Hobbs, 1977). However, computation of diffusional growth of a population of drops and droplet collection by stochastic processes necessitates explicit calculation of supersaturation and of the spectral distribution function of the number of drops. The amount of computation would strain the capacity of the most modern computers. Simplification or parameterization of the microphysical processes is obviously desirable.

Kessler (1969) proposed a parameterization scheme which partitioned all liquid water substance into cloud and precipitation. The latter is assumed to follow the Marshall–Palmer (1948) drop-size distribution at all times and to fall with a single effective fall velocity which depends only on the rainwater content and the height in the atmosphere. Interaction between cloud and rain is formulated on the concept of autoconversion of cloud to rainwater and accretion of cloud by falling raindrops. While Kessler's work significantly advanced the understanding of microphysical-kinematical interactions, certain limitations inherent in its simplicity have not been fully explored. In the first place, the Marshall–Palmer distribution may give a good estimate for average distributions which represent a large number of samples in many storms, but considerable departure from it occurs in individual cases (Mason and Andrews, 1960). Second, since the vertical transport of precipitation particles is related directly to the differential fallspeeds, a neglect of this aspect leads to improper distribution of hydrometeors which may in turn affect the circulation dynamics.

In an attempt to remove some of the restrictions in Kessler's parameterization but at the same time to avoid the large amount of computations required in a full stochastic scheme, a relatively simple model of microphysics is proposed. The gross features are as follows:

1) Cloud droplets are the direct consequence of condensation. As in Kessler's parameterization, only one category of cloud water is considered and detailed treatment of cloud-phase processes is omitted.

2) Kessler's autoconversion relation is used to model the process of stochastic collection of cloud droplets to form raindrop-size particles. However, autoconversion

[1] Present affiliation, Department of Meteorology, McGill University, Montreal.

0022-4928/79/040655-14$07.50

TABLE 1. Size categories for hydrometeors. In the model, 10 categories of raindrops are allowed while graupel categories extend from 1–15.

Type of hydrometeors	Range δR (cm)	Median radius R (cm)	Fall velocity V (m s^{-1})
Cloud	0–0.002	0.001	0.01
Rain and graupel categories			
1	0.002–0.008	0.005	0.23
2	0.008–0.04	0.025	1.95
3	0.04 –0.07	0.055	4.10
4	0.07 –0.10	0.085	5.74
5	0.10 –0.13	0.115	6.91
6	0.13 –0.16	0.145	7.73
7	0.16 –0.19	0.175	8.29
8	0.19 –0.22	0.205	8.66
9	0.22 –0.25	0.235	8.90
10	0.25 –0.28	0.265	9.06
11	0.28 –0.34	0.31	11.50
12	0.34 –0.46	0.40	13.00
13	0.46 –0.70	0.58	15.7
14	0.70 –1.18	0.94	20.0
15	1.18 –2.14	1.66	26.6

is assumed to produce only small raindrops $\sim 50\ \mu$m in radius. A Marshall–Palmer distribution is not imposed.

3) Evolution of particle-size spectra for rain and graupel and the effects of differential fall velocities are taken into account by partitioning rain and graupel particles into a total of 25 categories (Table 1). The mass distribution is computed rather than the spectral number density as in the stochastic method. A technique is developed for transferring mass from one category to another as hydrometeors grow or diminish in size.

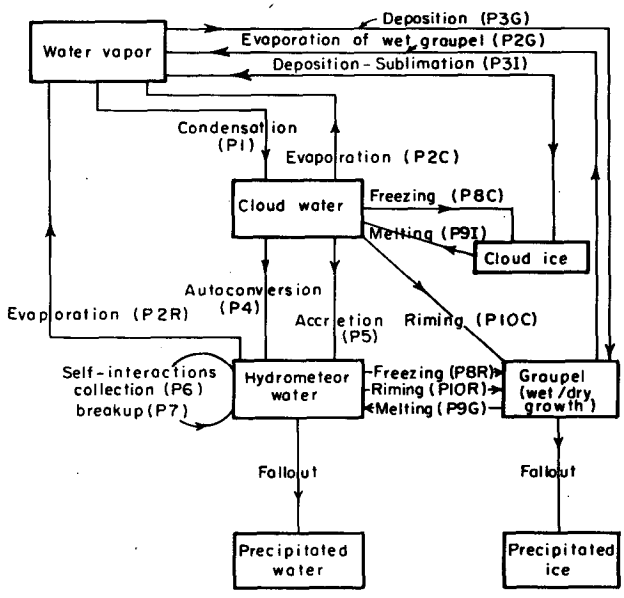

FIG. 1. The microphysical processes in the present (P) model. Precipitated water and precipitated ice refer to rain and graupel particles that fall onto the surface. Refer to text for P1, P2C, . . ., etc.

4) The processes of hydrometeor development which are modeled are evaporation, accretion, collection, breakup, freezing, riming, deposition and melting. The processes, their interactions and the symbols used to represent them are shown schematically in Fig. 1.

In Section 2 the model equations are formulated in three dimensions. In Section 3 the plausibility of the approach is established through comparison of results with other models in the context of a one-dimensional kinematic updraft. It is shown that for the development of warm rain the present model yields results comparable to those of a stochastic scheme. Section 4 contains sensitivity tests which indicate the extent to which the parameterization assumptions affect computations of the evolution of hydrometeor size spectra. A list of symbols is given in Appendix A.

2. Formulation of the model

a. *Continuity equations*

The mixing ratios for water vapor, cloud water and cloud ice obey continuity equations of the form

$$\frac{\partial \rho_0}{\partial t}\begin{bmatrix} q_v \\ q_c \\ \hat{q}_c \end{bmatrix} + \nabla\cdot\rho_0 \begin{bmatrix} q_v \\ q_c \\ \hat{q}_c \end{bmatrix}\mathbf{u} = \rho_0 \begin{bmatrix} \Phi_v \\ \Phi_c \\ \hat{\Phi}_c \end{bmatrix}$$

$$= \begin{bmatrix} -\mathrm{P1}+\mathrm{P2C}+\sum_R \mathrm{P2R}+\sum_R \mathrm{P2G}-\mathrm{P3I}-\sum_R \mathrm{P3G} \\ \mathrm{P1}-\mathrm{P2C}-\mathrm{P4}-\sum_R \mathrm{P5}-\mathrm{P8C}+\mathrm{P9I}-\sum_R \mathrm{P10C} \\ \mathrm{P3I}+\mathrm{P8C}-\mathrm{P9I} \end{bmatrix}. \quad (1)$$

The symbols on the right represent microphysical processes which act as sources and sinks; they are summarized in Table 2 and discussed in Section 2b.

Equations for the mixing ratios of rain and graupel for each group of particles with median radius R and range δR are

$$\frac{\partial \rho_0}{\partial t}\begin{bmatrix} q_r(R) \\ \hat{q}_r(R) \end{bmatrix} + \nabla\cdot\rho_0 \begin{bmatrix} q_r(R) \\ \hat{q}_r(R) \end{bmatrix}\mathbf{u} - \frac{\partial \rho_0}{\partial z}\begin{bmatrix} q_r(R) \\ \hat{q}_r(R) \end{bmatrix} V(R)$$

$$+\delta R \frac{\partial}{\partial R}\left\{\rho_0 \begin{bmatrix} q_r(R) \\ \hat{q}_r(R) \end{bmatrix}\frac{\dot{R}}{\delta R}\right\} = \rho_0 \begin{bmatrix} \Phi_r(R) \\ \hat{\Phi}_r(R) \end{bmatrix}$$

$$= \begin{bmatrix} -\mathrm{P2R}+\mathrm{P4}+\mathrm{P5}+\mathrm{P6}+\mathrm{P7_{sp}}+\mathrm{P7_{imp}} \\ -\mathrm{P8R}+\mathrm{P9G}-\mathrm{P10R} \\ -\mathrm{P2G}+\mathrm{P3G}+\mathrm{P8R}-\mathrm{P9G}+\mathrm{P10C}+\mathrm{P10R} \end{bmatrix}. \quad (2)$$

The last term on the left represents spectral shifting of drops from one size category to another as a result of the rate of change of radius brought about by the

microphysical processes. The last three terms on the left-hand side can be regarded as the divergence in a four-dimensional space with coordinates x, y, z and R.

The terminal velocities of raindrops are taken from measurements by Davies, reported by Best (1950). Graupel particles with a radius $\leqslant 0.265$ cm are assumed to fall with the same fallspeed as raindrops of similar size. For larger graupel, the equation by Mason (1971) is used, i.e.,

$$V(R)=\left(\frac{8}{3}\frac{\rho_g}{\rho_0}\frac{g}{C_D}R\right)^{\frac{1}{2}}. \tag{3}$$

The density of graupel is taken as 0.9 g cm^{-3} and the drag coefficient C_D is given the numerical value of 0.55 (English, 1973). The relatively high values for mass and fallspeed were selected as appropriate for hail-like graupel in summer convective storms or tropical showers. Recent measurements by Heymsfield (1978) suggest that somewhat lower values might be more suitable. Graupel in winter-type storms would probably be much less dense (Nakaya, 1954).

b. The microphysical processes

Formulation of the microphysical process is summarized in Table 2.

1) CONDENSATION, EVAPORATION AND SUBLIMATION (P1, P2, P3)

Clark (1973) computed the nucleation of cloud droplets from a spectrum of condensation nuclei and their subsequent growth by diffusion in a dynamic model. The cloud dynamics resulting from this detailed

TABLE 2. Summary of microphysical formulation.

Symbol	Process	Formulation	Reference
P1	Condensation	$\rho_0(q_v-q_s)\left[1+\frac{L_v^2 \quad q_s}{C_pR_v\ (\pi\theta)^2}\right]^{-1}$	Asai (1965)
P2C	Evaporation of cloud	Same as P1 with $q_v<q_s$	
P2R	Evaporation of rain	$-4\pi^*R(S-1)(1+0.21\ \mathrm{Re}^{\frac{1}{2}})N(R)\left[\frac{L_v}{\kappa T}\left(\frac{L_v}{R_vT}-1\right)+\frac{R_vT}{De_s(T)}\right]^{-1}$	Mason (1971)
P2G	Evaporation of graupel	$-2\pi^*R\hat{N}(R)(2.0+0.844\chi\ \mathrm{Re}^{\frac{1}{2}})D(\rho_v-\rho_{vG})$	English (1973)
P3I	Deposition or sublimation of cloud ice	$4\pi^*r(S_i-1)\hat{N}(r)\left[\frac{L_s}{\kappa T}\left(\frac{L_s}{R_vT}-1\right)+\frac{R_vT}{De_i(T)}\right]^{-1}$	Byers (1965)
P3G	Depositional growth of graupel	$2\pi^*R\hat{N}(R)(2.0+0.844\chi\ \mathrm{Re}^{\frac{1}{2}})D(\rho_v-\rho_{vG})$	English (1973)
P4	Autoconversion of cloud to rain	$K(\rho_0q_c-a)$ when $\rho_0q_c>a$ 0 otherwise	Kessler (1969)
P5R	Accretion of cloud by rain (gain in category R)	$N(R)\pi^*R^2V(R)E(R,r)\rho_0q_c$	Continuous collection process
P6	Collection of rain by rain	$\sum_{R'<R}N(R)\pi^*(R+R')^2[V(R)-V(R')]E(R,R')\rho_0q_r(R')$ $-\sum_{R'>R}N(R')\pi^*(R'+R)^2[V(R')-V(R)]E(R',R)\rho_0q_r(R)$	
$P7_{sp}$	Spontaneous breakup of raindrops	$-\rho_0q_r(R)P(R)+\sum_{R'>R}\rho_0q_r(R')P(R')Q(R',R)(R/R')^3$ For $P(R)$ and $Q(R',R)$ see Eqs. (5) and (6)	Srivastava (1971)
$P7_{imp}$	Breakup of raindrops by impaction	$-\sum_{R'\neq R}\tilde{N}_s(R,R')\left[\frac{0.06X(R)X(R')}{X(R)+X(R')}\right]$ $+\sum_{R'}\sum_{R''<R'}\tilde{N}_s(R',R'')\left[\frac{0.12X(R')X(R'')}{X(R')+X(R'')}\right]\delta_{R_s,R}$	Brazier-Smith *et al.* (1973)
P8C	Freezing of cloud drops	$\frac{\rho_0}{\delta t}\{\hat{q}_c[F(r,T)-1]+q_cF(r,T)\}$ For $F(r,T)$ see Eq. (9) and Table 3.	Danielsen *et al.* (1972)
P8R	Freezing of raindrops	$\frac{\rho_0}{\delta t}\{\hat{q}_r(R)[F(R,T)-1]+q_r(R)F(R,T)\}$ For $R(F,T)$ see Eq. (9) and Table 3.	Danielsen *et al.* (1972)
P9I	Melting of cloud ice	All melts at $T\geqslant 0$°C	
P9G	Melting of graupel	Heat transfer balance for dry or wet growth	English (1973)
P10C	Riming (cloud collected by graupel of size R)	$\hat{N}(R)\pi^*R^2V(R)E(R,r)\rho_0q_c$	
P10R	Riming (collection of rain)	$\sum_{R'<R}\hat{N}(R)\pi^*(R+R')^2[V(R)-V(R')]\hat{E}(R,R')\rho_0q_r(R')$	

treatment of nucleation and condensation do not deviate substantially from that of a bulk physical model where all supersaturated vapor condenses instantaneously. In view of this finding, condensation and evaporation of cloud droplets in the present model is computed from the dynamic effect alone. Modification of supersaturation mixing ratio through the release of latent heat in a manner proposed by Asai (1965) is adopted. The saturation excess $\delta M = q_v - q_s$ is calculated using Teten's formula [as given in Asai (1965)] to obtain q_s. A part of δM, δM_1, is condensed releasing latent heat which causes an increase in temperature; in turn, this permits the residue, $\delta M_2 = \delta M - \delta M_1$, to remain in vapor form. If the temperature is low enough so that cloud water freezes then $\hat{q}_s$ is used and the latent heat of sublimation is added to the air. Otherwise, in the presence of cloud, the air remains at water saturation. If $\delta M < 0$, the air is subsaturated and evaporation of cloud occurs; in this case $\delta M_1 =$ P2C and is taken from available cloud water.

If evaporation of all available cloud droplets still leaves the air subsaturated, evaporation of raindrops (P2R) and wet graupel particles (P2G) is allowed to occur. On the basis of experimental data by Macklin (1963), the numerical factor χ in the expression for P2G is assumed to be 0.7 for spherical graupel particles. In all of the formulations both cloud ice and graupel particles are assumed to be spherical.

2) Autoconversion (P4)

Autoconversion is assumed to produce only small raindrops with radii of $\sim 50\,\mu$m. Berry and Reinhardt (1974c) noted that the stochastic collection process tends to produce a natural break in the cloud-drop number density in the vicinity of $r = 40\,\mu$m, and suggested $50\,\mu$m as an appropriate division between rain and cloud droplets. In the present model a simple linear formulation is used for autoconversion rather than the more complicated relations derived by Berry (1968) and Cotton (1972). Yau (1973) found that Berry's functions for maritime and continental clouds can be closely matched by suitable choice of the constants in the linear formulation. Also, Silverman and Glass (1973) obtained similar cloud development in a one-dimensional time-dependent model with Kessler's and Berry's expressions for autoconversion.

3) Accretion, collection and riming (P5, P5R, P6, P10); collection efficiencies

The continuous collection process is assumed for accretion of cloud water by raindrops and graupel particles; formally it is also applied to collection of raindrops by larger water drops. It is recognized that during a given time step, raindrops of size R do not all grow in an identical mode. Any individual drop may collect a smaller drop, may coalesce with a larger drop or it may fail to experience a collision. The collection is essentially stochastic and only the probability for each type of event can be estimated. Here, however, we are not concerned with the development of individual drops but with the average rate at which water is being added to or removed from an ensemble of drops. The continuous collection assumption with appropriate collection efficiencies yields just such an average rate.

The collection efficiency for a drop of radius R collecting a smaller one of radius R', $E(R,R')$, is the product of collision and coalescence efficiencies, $E_1(R,R')$ and $E_2(R,R')$, respectively. Based on data from Mason (1971) it is assumed that for raindrops or graupel collecting cloud water the collision efficiency is 0.8 and coalescence efficiency is unity. For raindrops collecting raindrops, the collision efficiency is assumed to be unity but coalescence occurs only if the relative kinetic energy of the drops is small; otherwise, breakup ensues. Several experiments and analyses (Brazier-Smith *et al.*, 1972; Spengler and Gokhale, 1973; McTaggart-Cowan and List, 1975) led to similar conclusions regarding the probability of coalescence of raindrops. The formulation of Brazier-Smith *et al.* (1972) is used in this model:

$$E(R,R') = \frac{12\sigma^* f(R/R')}{5R'\rho_w[V(R) - V(R')]^2},$$

$$f(R/R') = f(\gamma) = \frac{[1+\gamma^2-(1-\gamma^3)^{\frac{1}{3}}][1+\gamma^3]^{11/3}}{\gamma^6(1+\gamma^3)}. \quad (4)$$

For collection of rainwater by graupel and hailstones a collection efficiency of unity is assumed. Experimental results from Macklin and Bailey (1968) indicate that the collection efficiency of smooth, solid spheres and artificial hailstones impacting on water drops decreases as the radius increases. The value can be as low as 0.2 for a stone with a radius of 4 cm. However, English (1973) compared the growth of hailstones in a modeled updraft using a collection efficiency of unity and the one given by Macklin and Bailey. She found that for stones with $R \leqslant 1.25$ cm the difference in final diameter was not important. Since the largest graupel in the present model is 1.66 cm, a collection efficiency of unity seems appropriate.

For collisions involving only ice particles (graupel with cloud ice or smaller graupel) it is assumed that the particles do not adhere and the collection efficiency is zero.

4) Breakup ($P7_{sp}$, $P7_{imp}$)

The problem of drop breakup by aerodynamic instability on free fall was studied by Komayabasi *et al.* (1964) and Srivastava (1971). The expression for the probability of breakup and the size distribution of the

fragments are

$$P(R)=2.94\times10^{-7}\exp(34R)\ [\text{s}^{-1}], \quad (5)$$

$$Q(R_0,R)=\frac{436.1}{R_0}\exp(-7R/R_0)\ [\text{cm}^{-1}]. \quad (6)$$

Eq. (5) indicates that spontaneous breakup is negligible except for very large drops, $\gtrsim 0.25$ cm in radius. Since $R=0.265$ cm is the maximum size for water drops in the present model, it is assumed that drops which exceed this size break up instantaneously and are redistributed according to (6).

A breakup mechanism of considerably greater importance is impaction. Experiments by Whelpdale and List (1971), Spengler and Gokhale (1973), Brazier-Smith *et al.* (1972) and McTaggart-Cowan and List (1975) indicate that a variety of modes of breakup often result when raindrops collide. In general, impaction results in distributions of water masses which peak around the original sizes of the parent drops. But formation of satellites appears to play a non-negligible role in shaping the size distribution of precipitation (Young, 1975; List and Gillespie, 1976).

To include the effects of drop breakup and the formation of satellites, the simple model of Brazier-Smith *et al.* (1973) is adopted. Each collision between drops of masses $X(R)$ and $X(R')$ is assumed to produce three satellite drops of radius R_s and mass $0.04X(R)X(R')/[X(R)+X(R')]$, contributed equally by each of the colliding pair. Fig. 2 shows the sizes of the satellite drops produced and points up the dominant role of the smaller drops in determining the size of the satellites.

The number of collisions, per unit volume and time interval, that occur between drops of radius R and R' is

$$\tilde{N}(R,R')=\pi^*(R+R')^2E_1(R,R')N(R)N(R')\times[V(R)-V(R')]. \quad (7)$$

The number of separations is given by

$$\tilde{N}_s(R,R')=\tilde{N}[1-E_2(R,R')]. \quad (8)$$

Therefore, the mass of water lost from each category of radius R and R' is

$$\tilde{N}_s(R,R')\frac{0.06X(R)X(R')}{X(R)+X(R')}$$

and the mass of satellites produced is

$$\tilde{N}_s(R,R')\frac{0.12X(R)X(R')}{X(R)+X(R')}.$$

In Table 2, $P7_{sp}$ represents spontaneous breakup and $P7_{imp}$ breakup caused by impaction. $\delta_{R_s,R}$ is a Dirac delta function.

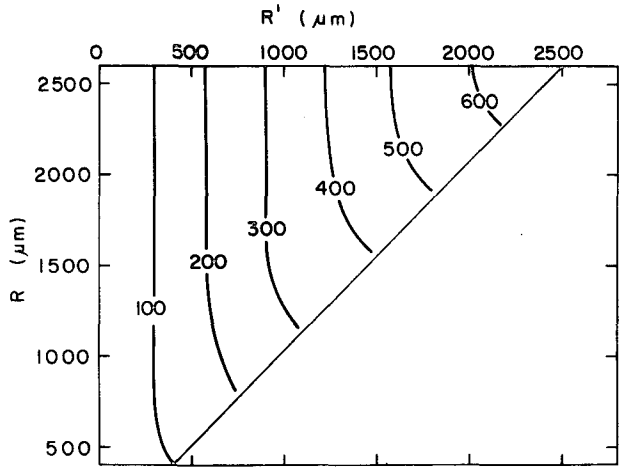

FIG. 2. Radius (R_s) of satellite drops produced by impaction of drops of radii R and R' ($R>R'$). The contours of R_s are in micrometers.

5) FREEZING (P8C, P8R)

Mechanisms for initiation of the ice phase are still poorly understood. Bigg (1953) and Vali (1968) considered the probability of freezing with the assumption that freezing nuclei are contained within the water droplets. Young (1974a) examined ice particle multiplication mechanisms and proposed a model of ice phase nucleation based on contact nucleation. However, no direct measurement of contact nuclei is available and the exact mechanism for this process remains controversial (Fukuta, 1975; Cooper, 1975). In view of this situation, a highly simplified model is adopted and sensitivity tests are used to give insight into the freezing processes.

Based on Vali's (1968) observation of the freezing of water drops formed from bulk precipitation samples, Danielsen *et al.* (1972) suggested a simple formula for the rate at which freezing nuclei are activated as droplets are cooled below 0°C. Integration of their formula yields $F(v)$, the fraction of drops of volume v frozen at temperature T(°C):

$$F(v)=1-\exp[-vK_1(T)], \quad (9)$$

where

$$K_1=\begin{cases}1.47\{\exp[-0.68(T+7)]-1\}, & \text{for } T<-7°\text{C}\\ 0, & \text{for } T>-7°\text{C}.\end{cases}$$

This fraction as a function of temperature and median radius is listed in Table 3. The median radius of cloud particles is assumed to be 10^{-3} cm.

In the present model it is assumed that at temperatures below −7°C the fraction of particles of volume v which are frozen is at least $F(v)$ as given in (9). Therefore, freezing occurs whenever, in any individual particle-size category, the ratio of the mass of graupel to the total mass of rain plus graupel is less than $F(v)$.

TABLE 3. Fraction of drops of radius R frozen at temperatures T (°C).

T (°C)	R (cm) 0.001	0.005	0.025	0.055	0.085	0.115	0.145	0.175	0.205	0.235	0.265
−10	4.5×10^{-8}	5.1×10^{-6}	6.4×10^{-4}	6.8×10^{-3}	2.5×10^{-2}	6.1×10^{-2}	0.12	0.20	0.30	0.41	0.53
−15	1.4×10^{-6}	1.8×10^{-4}	2.2×10^{-2}	0.21	0.58	0.88	0.98	1	1	1	1
−20	4.3×10^{-5}	5.3×10^{-3}	0.49	1	1	1	1	1	1	1	1
−25	1.3×10^{-3}	0.15	1	1	1	1	1	1	1	1	1
−30	3.7×10^{-2}	0.99	1	1	1	1	1	1	1	1	1
−35	0.68	1	1	1	1	1	1	1	1	1	1
−40	1	1	1	1	1	1	1	1	1	1	1
−45	1	1	1	1	1	1	1	1	1	1	1

The formulations for P8R and P8C in Table 2 refer to an average rate of freezing in a time step δt. For simplicity, frozen drops are assumed to remain spherical with a density of 1 g cm^{-3}, i.e., the mass frozen at any time step is transferred from water category to ice category for particles of the same size.

6) GROWTH MODE OF GRAUPEL AND MELTING (P9G, P9I)

Often all of the supercooled water collected by graupel cannot be frozen as the particle is warmed by latent heat released during the freezing process. The modes of growth of graupel particles and the rate of melting of the ice core are determined from the heat transfer equation of English (1973). It is assumed that the graupel content in each size category has an ice portion $\hat{q}_{ri}$ and a water portion $\hat{q}_{rw}$. Water may be added by collection or lost by evaporation; ice may be added or lost by sublimation. Under equilibrium conditions, heat transfers by conduction and convection produce a balance between the heat generated by freezing and deposition and the sensible heat required to bring the temperature of the collected water to the surface temperature of the graupel. If freezing all of the available water does not raise the temperature above 0°C, then a dry mode of growth is assumed. Otherwise, only enough water is frozen or melted to bring the particle temperature to 0°C.

Transfer of graupel particles to raindrops is made when $\rho_0\hat{q}_{ri}\lesssim 0$.

c. *Computational procedures*

In (1) and (2) all of the processes which tend to increase or diminish the water substances in any of the cloud, vapor or hydrometeor categories are included. In nature these processes go on at the same time, so that ideally the equations should be solved simultaneously as written. Some simplifications have been introduced into the actual computations, however, and the adopted sequence of calculation is as follows:

1) Using the median radius R, the change of water mass (dm) in each rain category through autoconversion (P4), collection (P5, P6, P10R), and breakup ($P7_{sp}$, $P7_{imp}$) is determined. $\dot{R}$ is then obtained from dm and is used to compute the shifting term using a special technique developed by Egan and Mahoney (1972). This technique, as described in Appendix B, involves calculations of the first and second moments of the distribution within each size category. It avoids numerical spreading of the spectra although it may tend to suppress spectral spreading caused by the stochastic nature of the collection and breakup processes. In any case, it results in more realistic spectra than those obtained with simple finite-differencing techniques. With the latter, the rate at which some rainwater appears in progressively larger size categories depends on the magnitude of the time step, and unrealistically rapid appearance of large drops may result.

2) For temperatures below 0°C, the sublimation of cloud ice (P3I) is calculated assuming a radius of 10 μm and a saturation with respect to ice at the ambient temperature. The vapor field is adjusted accordingly.

3) The rates of mass change in each graupel category through sublimation (P3G) and riming (P10C, P10R) are utilized in the heat transfer equation to determine the growth mode of the graupel particles. For sufficiently warm temperatures, the heat transfer equation also gives the rate of melting of the ice core. If the ice portion of the graupel turns out to be zero, complete melting of the graupel (P9G) into rain would take place. The Egan and Mahoney technique is again invoked to compute the shifting term.

4) Instantaneous melting of cloud ice (P9I) occurs if the temperature T is warmer than 0°C. For $T<-7$°C, freezing (P8C, P8R) of cloud and rain water, proceed at a rate determined by the ambient temperature and the ratio of the mass of graupel (or cloud ice) to the mass of rain water (or cloud water) in the same size category.

5) Condensation (P1) or evaporation of cloud water (P2C) and evaporation of rain particles (P2R) complete the computation sequence.

3. Comparison of the present model with other schemes

a. *Nature of comparisons*

The present microphysical model differs from the Kessler parameterization and the stochastic method

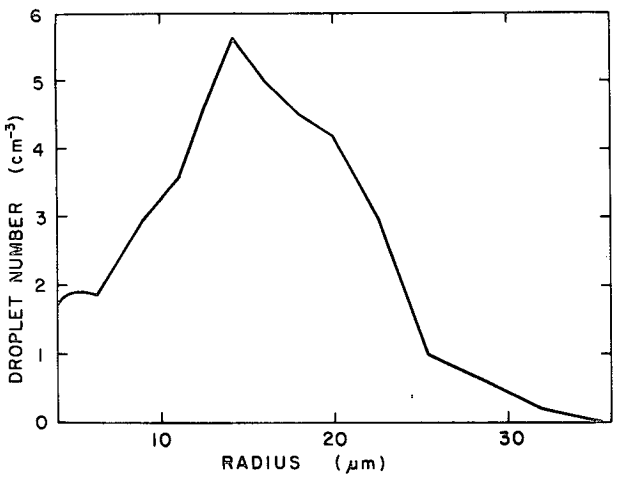

FIG. 3. The initial droplet spectrum for model S.

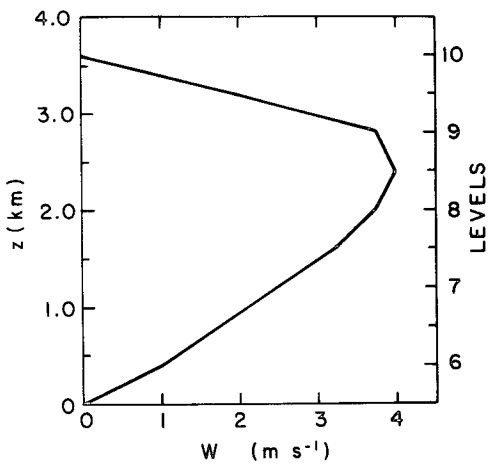

FIG. 4. The kinematic updraft profile.

mainly in the assumption about autoconversion and the calculation of the collection processes. As such, it will be tested in a situation where these processes are included. Specifically, the effects of the initiation of warm rain in a one-dimensional kinematic updraft are compared. For the stochastic method (model S), the formulation by Nelson (1971) is used. The Kessler model (model K) follows Kessler's (1969) formulation, but in order to compare with model S the condensation and evaporation terms are omitted. Similarly, for this present model (model P) only autoconversion, collection, spontaneous breakup and rainout are included. For all three models computations are made under identical conditions as are in Nelson (1971).

The vertical dimension in the domain is represented by 10 space levels. In accordance with the initial condition used by Nelson, a cloud water content of 0.8 g m^{-3} is specified at levels 2–10 for models P and K. Level 1 is retained as a rainout accumulator to conserve the total mass within the system. The initial drop-size spectrum for model S (shown in Fig. 3) was obtained from observational data of Braham *et al.* (1957) in tropical cumuli. The updraft profile used in the calculations is shown in Fig. 4.

The vertical transport terms are solved by a forward upstream method with $\delta t = 20$ s and $\delta z = 400$ m. Reduction of δt to half this value does not significantly change the results.

b. Results

The evolution of the liquid water content, surface rainfall rate, radar reflectivity profile and drop-size spectra are compared for the three models. Results are shown in Figs. 5–8. It can be seen that the behavior of

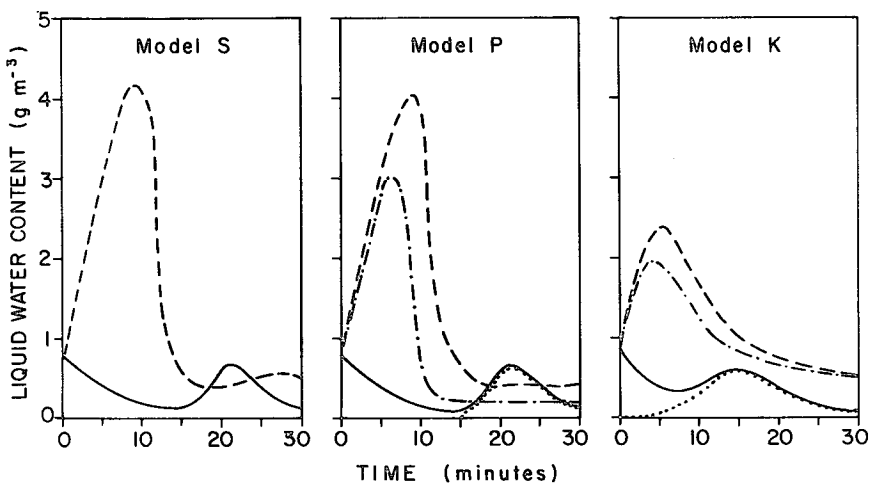

FIG. 5. Comparison of liquid water for models S, P and K. Cloud + rain water at 400 m (solid line); at 3200 m (dashed line); cloud water at 3200 m for models P and K (dashed-dotted line); rain water at 400 m for models P and K (dotted line).

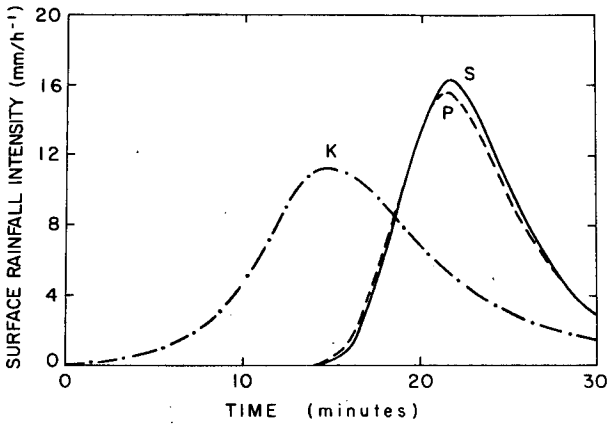

FIG. 6. Comparison of surface rainfall intensity for models S, K and P. $a=0.5$ g m^{-3}, $K=10^{-3}$ s^{-1}.

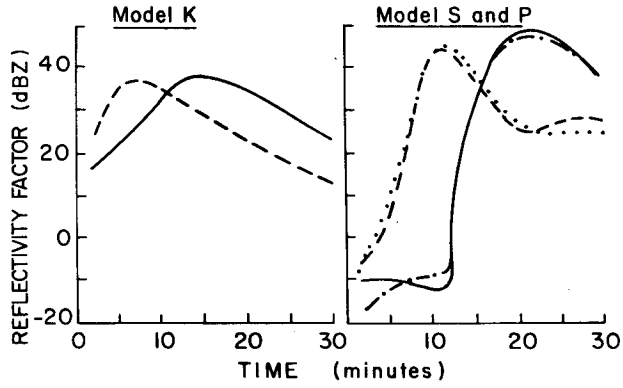

FIG. 7. Comparison of radar reflectivities at 400 m and 3200 m. Models S and K at 400 m (solid line), 3200 m (dashed line); model P at 400 m (dashed-dotted line), 3200 m (dotted line).

all the quantities is almost identical for the stochastic (S) and present (P) models. The curves resulting from the Kessler (K) model are generally similar in shape to the others, but significant differences in the magnitudes of the quantities and in the timing are observed. These differences can be attributed primarily to the fact that in the early stages of rain formation the drops tend to be larger and to fall faster in the K model than in the others. For example, in Fig. 5 all of the models develop accumulations of liquid water at 3200 m, above the updraft maximum, after approximately 7 min. In the K model, however, with its faster falling raindrops the maximum is less pronounced and occurs earlier than in the P and S models. The earlier depletion of cloud water and more rapid precipitation fallout leads to considerably less rain water near cloud base at a later time.

Time profiles for surface rainfall rate (Fig. 6) and radar reflectivity factor (Fig. 7) are very similar for models P and S. Model K produced an earlier rainfall maximum and a lower peak reflectivity factor.

The evolution of raindrop-size spectra for models S and P at 18, 22 and 26 min is shown in Fig. 8. Except for a slight scarcity of drops around 500 μm radius at the cloud base and a narrower spectrum at 18 min, model P agrees closely with the stochastic model.

The realism of the one-dimensional stochastic model in simulation of the warm rain process has been discussed by Nelson (1971). He concluded that despite neglect of horizontal divergence it gives results consistent with the observed liquid water content and the onset of rain in tropical cumuli. The present microphysical scheme has been shown to give comparable results in terms of liquid water content, rainfall rate, radar reflectivity profiles and size spectra of raindrops. Therefore, it represents a desirable alternative to the stochastic scheme on account of the small volume of computations required.

4. Sensitivity tests

Various sensitivity tests that have been performed with model P are listed in Table 4. For these tests the updraft profile in Fig. 4 was assumed and condensation and evaporation processes were omitted. Except for

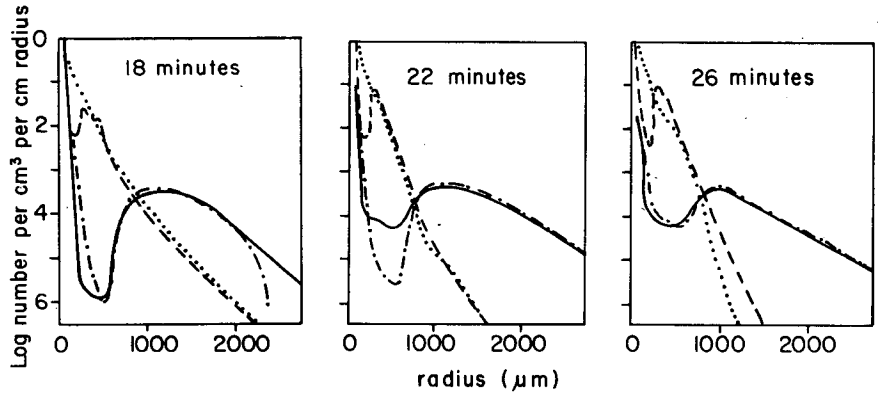

FIG. 8. The evolution of raindrop size spectra for models S and P at 18, 22 and 26 min. Model S spectrum at 400 m (solid), 3200 m (dashed); model P spectrum at 400 m (dashed-dotted), 3200 m (dotted).

TABLE 4. Sensitivity tests performed.

Process	Quantity	Tests
Autoconversion	Autoconversion rate (K)	$K=10^{-2}$ s^{-1}
		$K=10^{-3}$ s^{-1} with $a=0.5$ g m^{-3}
		$K=10^{-4}$ s^{-1}
	Autoconversion threshold (a)	$a=0$ g m^{-3}
		$a=0.7$ g m^{-3} with $K=10^{-3}$ s^{-1}
Collection (rain-rain)	Self collection of rain particles	Self-collection of rain, particles allowed
		Self-collection of rain, particles not allowed
	Coalescence efficiency $E_2(R,R')$ and satellite drops	$E_2(R,R')=1$, no satellite drops
		$E_2(R,R')$ from Brazier-Smith *et al.* (1973), no satellite drops
		$E_2(R,R')$ from Brazier-Smith *et al.* (1973), with satellite drops
Freezing melting, and riming	Temperature of the updraft	Temperature profiles $T_1(z)$, $T_2(z)$, $T_3(z)$ as listed in text

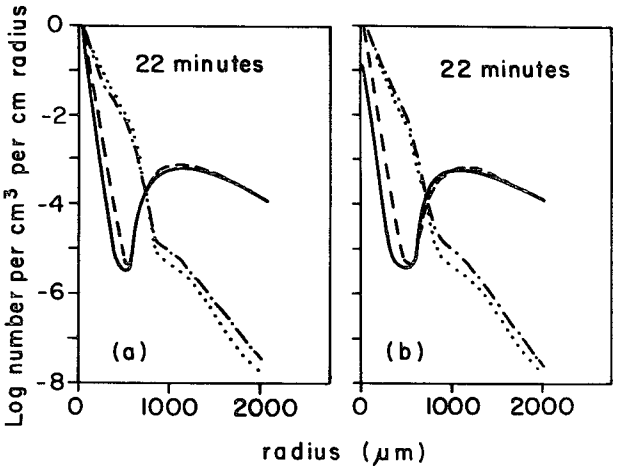

FIG. 10. Effect on raindrop-size spectra of varying autoconversion parameters. (a) $a=0.5$ g m^{-3}. Spectrum at 400 m, $K=10^{-3}$ s^{-1} (solid), $K=10^{-2}$ s^{-1} (dashed). Spectrum at 3200 m, $K=10^{-3}$ s^{-1} (dotted-dashed), $K=10^{-2}$ s^{-1} (dotted). (b) $K=10^{-3}$ s^{-1}. Spectrum at 400 m, $a=0.7$ g m^{-3} (solid), $a=0$ (dashed). Spectrum at 3200 m, $a=0.7$ g m^{-3} (dotted-dashed), $a=0$ (dotted).

the autoconversion tests, values of $a=0.5$ g m^{-3} and $K=10^{-3}$ s^{-1} were used. Ice phase processes were not included except in the third group of tests.

a. Effect of autoconversion rate and threshold

Because the selection of values for autoconversion rate and threshold is rather arbitrary, sensitivity tests were run to determine the effects of different choices for these parameters. The results in Figs. 9–11 indicate that the development of precipitation is relatively insensitive to changes in a and K. This insensitivity is not surprising since the combined effect of autoconversion and collection is responsible for growth of precipitation in this model. Any increase (decrease) of

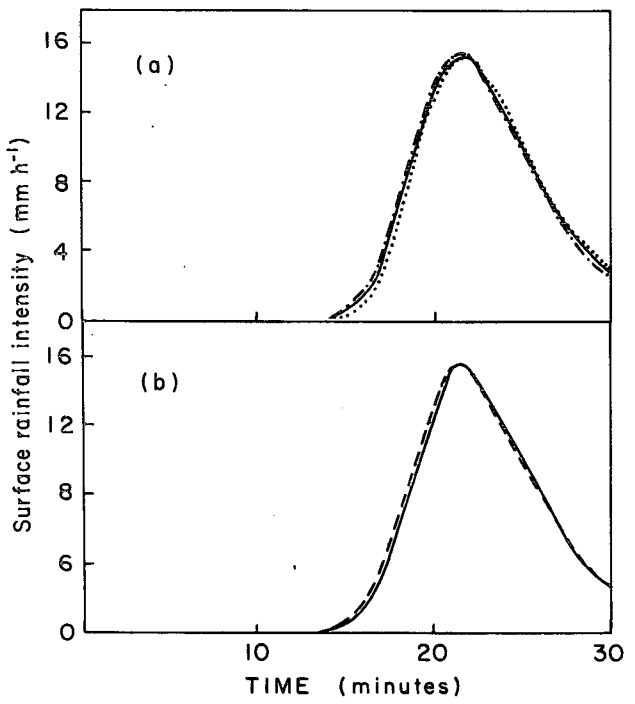

FIG. 9. Effect on rainfall intensity of varying autoconversion parameters in model P. (a) $a=0.5$ g m^{-3}, $K=10^{-4}$ s^{-1}, (dotted), 10^{-3} s^{-1} (solid), 10^{-2} s^{-1} (dashed-dotted); (b) $K=10^{-3}$ s^{-1}, $a=0$ (dashed), 0.7 g m^{-3} (solid).

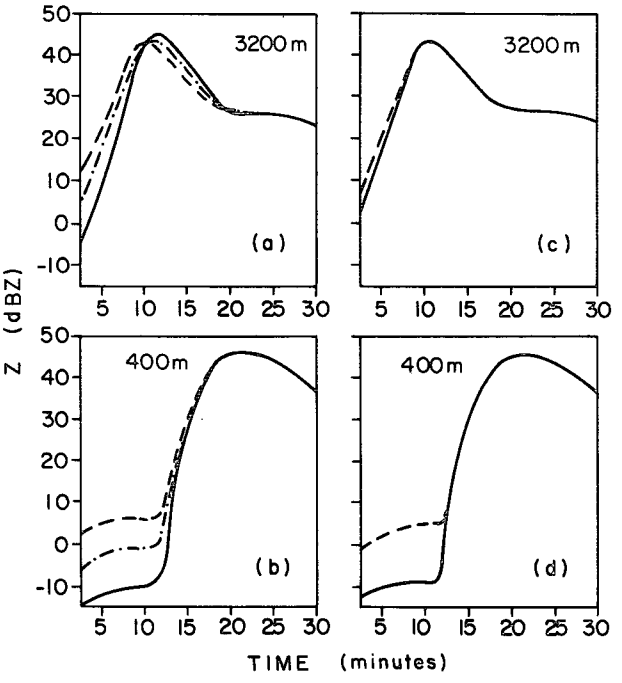

FIG. 11. Effect on radar reflectivity of varying autoconversion parameters. (a) and (b): $a=0.5$ g m^{-3}; $K=10^{-4}$ s^{-1} (solid), 10^{-3} s^{-1} (dotted-dashed) 10^{-2} s^{-1} (dashed); (c) and (d): $K=10^{-3}$ s^{-1}; $a=0.7$ g m^{-3} (solid), 0 (dashed).

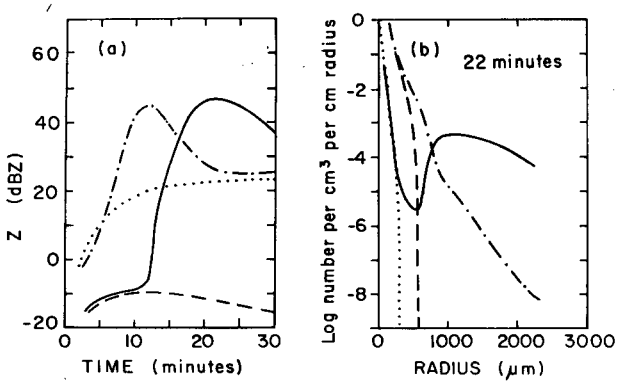

FIG. 12. Effect of rain-rain interaction (R-R) on time evolution of radar reflectivity factor (Z) and drop-size spectrum. (a) Z at 400 m, with R-R (solid), no R-R (dashed); Z at 3200 m, with R-R (dotted-dashed), no R-R (dotted). (b) Drop-size spectrum at 400 m, with R-R (solid), no R-R (dashed); drop-size spectrum at 3200 m, with R-R (dotted-dashed), no R-R (dotted).

the rate of the autoconversion process decreases (increases) the cloud water content which in turn decreases (increases) the accretion rate for cloud droplets. Thus as one process is enhanced the other diminishes, and the development of precipitation through the combination of the two is not greatly affected.

It is probable that this insensitivity would be modified if condensation, evaporation and horizontal divergence were included. Nevertheless, model P is expected to be less sensitive to the autoconversion process than model K. The reason is that in the former case, autoconversion produces only small raindrops centered at 50 μm radius.

b. *Effect of rain-rain interaction*

The importance of rain-rain interactions, which has been pointed out by Berry and Reinhardt (1974, b), is illustrated in Fig. 12. Suppression of this effect leads to a much slower growth process with negligible rainfall at the surface. The maximum size of the particles at cloud base is limited to 300 μm and the radar reflectivity factor never exceeds 25 dBZ. This demonstrates that the process of accretion of only cloud drops is inadequate to explain observed size spectra. Raindrop interactions stand out as a major mechanism in the development of precipitation.

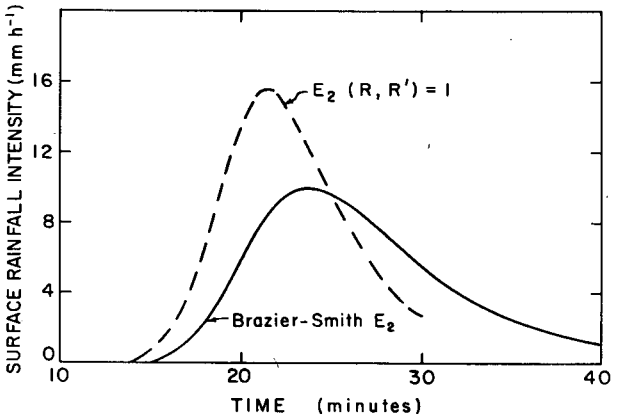

FIG. 13. Effect of coalescence efficiency on rainfall intensity. The case including satellite drops with Brazier-Smith coalescence efficiency shows no difference from the solid curve.

c. *Effects of coalescence efficiency and satellite drops*

List and Gillespie (1976) have emphasized the importance of impaction breakup as a limiting mechanism for the growth of large drops. The importance of this effect is illustrated in Figs. 13 and 14 which show rainfall rate, radar reflectivity and drop-size spectra computed with the coalescence efficiencies in Table 3 and with unit coalescence efficiency. The narrower drop-size spectrum resulting from the impaction breakup causes a delay of the onset of rainfall and a smaller maximum rainfall rate. Radar reflectivity near the cloud base is generally smaller; a difference of 6 dBZ appears at a time of 21 min.

Calculations including and omitting the formation of satellite drops indicate that the rainfall rate and radar reflectivity factor are relatively insensitive to the formation of satellite drops. The major effect of satellites is to cause a slight but perceptible increase in the spectral number density for drops <500 μm. Young (1975) reached a similar conclusion from his calculations.

d. *Effects of including ice phase*

The primary purpose of the test is to determine qualitatively how the inclusion of ice processes would affect the evolution of precipitating particle size spectra. The results are probably not quantitatively realistic because of freezing in cumulus cells is not yet fully understood and the present parameterization is extremely simplified. As the kinematic model does not treat the vapor phase explicitly, only freezing, riming

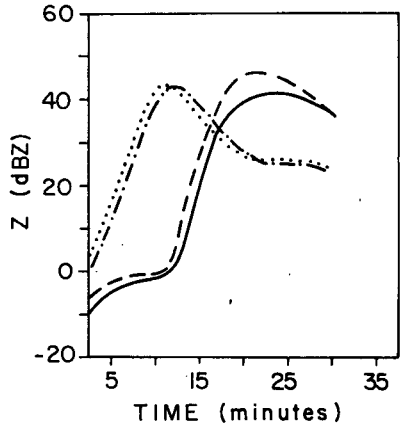

FIG. 14. Effect of coalescence efficiency and satellites on radar reflectivity profile (Z).

$E_2=1$: at 3200 m (dotted), at 400 m (dashed)
E_2, Brazier-Smith: at 3200 m (dotted-dashed), at 400 m (solid)

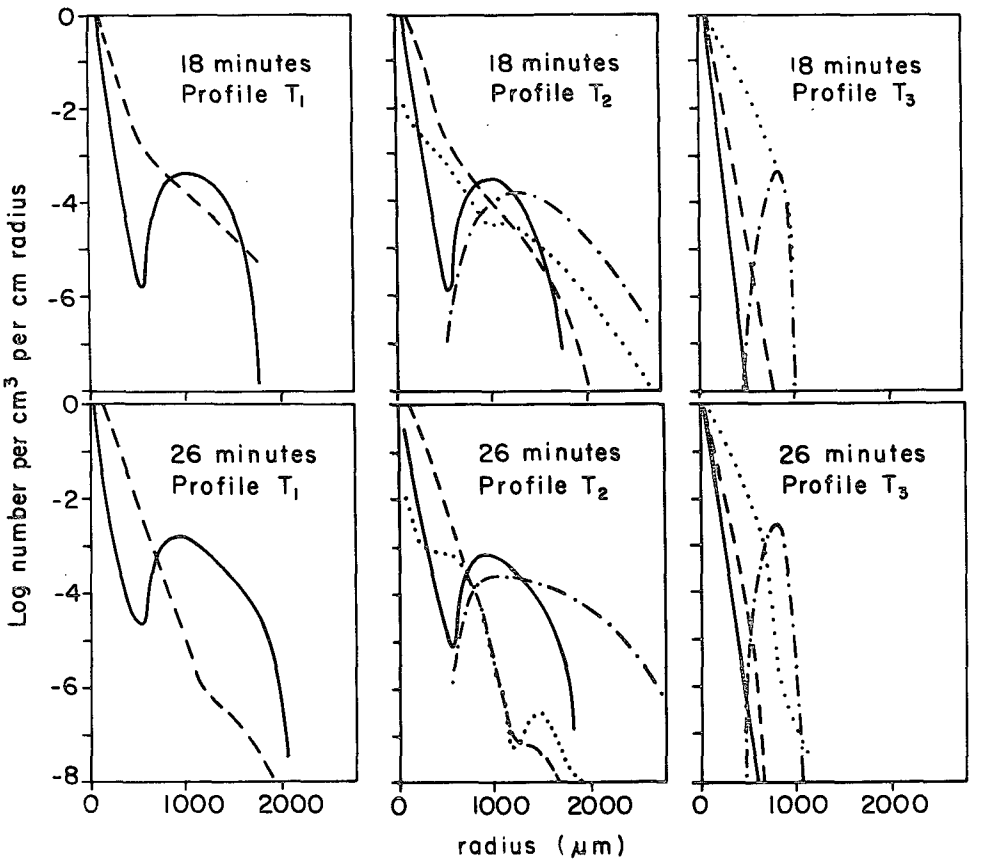

FIG. 15. Raindrop and graupel size spectra for temperature profiles T_1, T_2 and T_3 as described in text. Rain at 400 m (solid), at 3200 m (dashed); graupel at 400 m (dotted-dashed), at 3200 m (dotted).

and melting are considered; deposition and evaporative processes are omitted. The temperature in the updraft affects directly the rate of the ice phase processes and therefore constitutes an important parameter. The development of precipitation is computed for three linear temperature profiles, with lapse rates of 6.3°C km^{-1}. The freezing and melting levels (−7 and 0°C, respectively) and surface temperatures are listed below:

Temperature profile	$T_1(z)$	$T_2(z)$	$T_3(z)$
Freezing level (km)	3.4	2.2	1.1
Melting level (km)	2.2	1.1	0
Surface temperature (°C)	14.0	7.0	0

The evolution of rain and graupel size spectra for T_1, T_2 and T_3 are shown in Fig. 15. Freezing occurs very near the cloud top in T_1 on account of the high freezing level, and only a minute quantity of small graupel forms. The raindrop-size spectra remain similar to those of the nonfreezing case. With the freezing level at 2.2 km in T_2, the graupel particles form mostly above the updraft maximum and grow rapidly from the accumulation of supercooled water drops. Comparison of the precipitation spectra in Fig. 15 indicates that with T_2 the growth of graupel particles significantly broadens the precipitation particle size distributions both near the cloud top and near the cloud base. However, the raindrop spectrum is somewhat narrower. For T_3, rapid freezing occurs throughout most of the updraft, and narrow spectra result for both the rain and graupel particles. The depletion of supercooled water due to the rapid freezing and the presence of numerous small graupel particles, which in this model are not collected, slows down the precipitation growth rate.

It appears, therefore, that a moderate freezing rate together with a supply of supercooled water enhances the development of graupel particles. Rapid freezing, however, with depletion of supercooled water can slow down the growth of both graupel and rain.

5. Conclusion

A method has been presented for parameterizing the microphysical processes in a cumulus cell. This method overcomes many of the limitations of the very simple Kessler parameterization, and it allows computation of the development of particle-size spectra and the distribution of radar reflectivity in model cells. We have shown that in the absence of the ice phase the resulting drop-size spectra are almost identical with those ob-

tained by the much more detailed stochastic method, although they are achieved with considerably less computation load. Although the parameterization of the ice-phase processes is extremely simplified, its usefulness in providing insight into the effects of glaciation has been demonstrated.

The proposed parameterization scheme is especially useful for comparing the characteristics of model cells with those of actual cells which have been observed by radar, since the development of particle-size spectra is considerably more realistic than with the Kessler parameterization. In a future paper the effect of microphysical parameterization on the development of dynamic cell models will be considered.

Acknowledgments. The research described in this paper was supported by the National Science Foundation under Grant GA 36364X1 and by the National Oceanic and Atmospheric Administration under Grant 04-5-022-1.

APPENDIX A

List of Symbols

a	threshold for autoconversion (g cm^{-3})
C_p	specific heat of air at constant pressure (1.004×10^7 cm^2 s^{-2} K^{-1})
C_D	drag coefficient of graupel in air (0.55)
D	coefficient of molecular diffusion of water vapor in air (0.24 cm^2 s^{-1})
e_s	saturation vapor pressure with respect to water
e_i	saturation vapor pressure with respect to ice
E	collection efficiency for water drops
E_1	collision efficiency for water drops
E_2	coalescence efficiency for water drops
$\hat{E}$	collection efficiency for graupel impacting on water drops
g	gravitational acceleration (980 cm s^{-2})
K	rate of autoconversion (s^{-1})
L_v	latent heat of condensation or evaporation (2.5×10^{10} cm^2 s^{-2} K^{-1})
L_f	latent heat of fusion (0.334×10^{10} cm^2 s^{-2} K^{-1})
L_s	latent heat of sublimation (2.83×10^{10} cm^2 s^{-2} K^{-1})
N	concentration of water particles (cm^{-3})
$\hat{N}$	concentration of ice particles (cm^{-3})
$\tilde{N}$	number of collisions between raindrops (cm^{-3} s^{-1})
$\tilde{N}_s$	number of separations after collision (cm^{-3} s^{-1})
P1, P2, etc.	microphysical processes summarized in Table 2
$P(R)$	probability of spontaneous breakup (s^{-1})
$Q(R_0,R)$	drop-size distribution for spontaneous breakup (cm^{-1})
q_v	vapor mixing ratio of air
q_s	saturation vapor mixing ratio of air (with respect to water)
$\hat{q}_s$	saturation vapor mixing ratio of air (with respect to ice)
q_c	cloud water mixing ratio of air
$\hat{q}_c$	cloud ice mixing ratio of air
q_r	rain water mixing ratio of air
$\hat{q}_r$	graupel mixing ratio of air
$\hat{q}_{ri}$	ice portion of graupel mixing ratio
$\hat{q}_{rw}$	water portion of graupel mixing ratio
r	radius of cloud drop (cm or μm)
R	radius of raindrop (cm)
$\dot{R}$	rate of change of radius (cm s^{-1})
R', R''	radius of raindrop used as integration or summation variable (cm)
$\hat{R}$	radius of graupel particle (cm)
R_v	gas constant for water vapor (4.6×10^6 cm^2 s^{-2} K^{-1})
Re	Reynold's number
S	saturation ratio over water
S_i	saturation ratio over ice
t	time (s)
T	temperature (K or °C)
$\mathbf{u}$	velocity of air in three dimensions (cm s^{-1})
v	volume of a raindrop (cm^3)
V	terminal fall velocity of hydrometeors (cm s^{-1})
X	mass of one drop (g)
δR	the spread of each size category (cm)
δt	time step (s)
δz	space step (cm)
∇	three-dimensional del operator
θ	potential temperature (K)
κ	thermal conductivity of air (2.4×10^3 g cm s^{-3} K^{-1})
ν	kinematic viscosity of air (0.15 cm^2 s^{-1})
π^*	3.14159
π	dimensionless pressure unit
ρ_g	density of graupel (g cm^{-3})
ρ_0	base-state air density (g cm^{-3})
ρ_{vG}	vapor density at surface of graupel (g cm^{-3})
ρ_v	vapor density of environment (g cm^{-3})
ρ_w	density of water (g cm^{-3})
σ^*	surface tension of water drops (g s^{-2})
Φ_c	total sources and sinks for cloud water
$\hat{\Phi}_c$	total sources and sinks for cloud ice
Φ_r	total sources and sinks for rainwater
$\hat{\Phi}_r$	total sources and sinks for graupel
Φ_v	total sources and sinks for water vapor
χ	numerical factor used in heat transfer coefficient

APPENDIX B

Technique for Spectral Shifting

This appendix describes the procedure for applying the E & M technique (Egan and Mahoney, 1972) in

calculating the spectral shifting of rain and graupel masses from one size category to the next. Application of the method involves calculations of the first and second moments of the hydrometeor mass distribution after transfer has been made into and out of a particular category. The first moment represents the center of mass and the second moment is taken to be a measure of the horizontal spread. A new rectangular distribution is then reconstructed having the same hydrometeor water content and identical first and second moments as those computed.

Fig. 16 illustrates the computation using this procedure. The hydrometeor water in the mth category is assumed to be distributed in a rectangular block with a transformation of coordinates which places 0 at the center and a value of 0.5 and -0.5 at the ends of the range interval. All length scales in a category are normalized to its range δR_m.

Let $(\rho_0 q_r)^n_{mj}$, F^n_{mj}, H^n_{mj}, R^n_{mj} be the water content, center of mass, height and spread of the distribution for the mth category at a grid point j and time step n. In this coordinate system then

$$(\rho_0 q_r)^n_{mj} = H^n_{mj} R^n_{mj}.$$

The change of radius in a time step, $\dot{R}_m \delta t$, computed as described in Section 2c, advances the center of mass by a distance σ given by

$$\sigma = \frac{\dot{R}_m \delta t}{\delta R_m}.$$

In this example σ is assumed positive. The case for negative σ can be obtained using the same reasoning. A portioning parameter

$$P^n_{mj} = (F^n_{mj} + \sigma + \tfrac{1}{2} R^n_{mj} - 0.5)/R^n_{mj}$$

is then calculated. For $P^n_{mj} < 0$, none of the water is transferred. For $P^n_{mj} > 1$ all the water is transferred into the upper category. For $1 > P^n_{mj} > 0$, an amount $P^n_{mj}(\rho_0 q_r)^n_{mj}$ is transferred to category $m+1$ and $(1-P^n_{mj})(\rho_0 q_r)^n_{mj}$ remains. The water transferred to an upper category will have a center of mass at

$$0.5\left(P^n_{mj} R^n_{mj} \frac{\delta R_{m+1}}{\delta R_m} - 1\right)$$

relative to the center of the $m+1$th category and a spread equal to

$$P^n_{mj} R^n_{mj} \frac{\delta R_m}{\delta R_{m+1}}.$$

For the water remaining in the mth category, its center of mass and spread are, respectively,

$$(1 - R^n_{mj} + P^n_{mj} R^n_{mj})/2 \quad \text{and} \quad (1 - P^n_{mj}) R^n_{mj}.$$

For the general case of transfer into and out of a

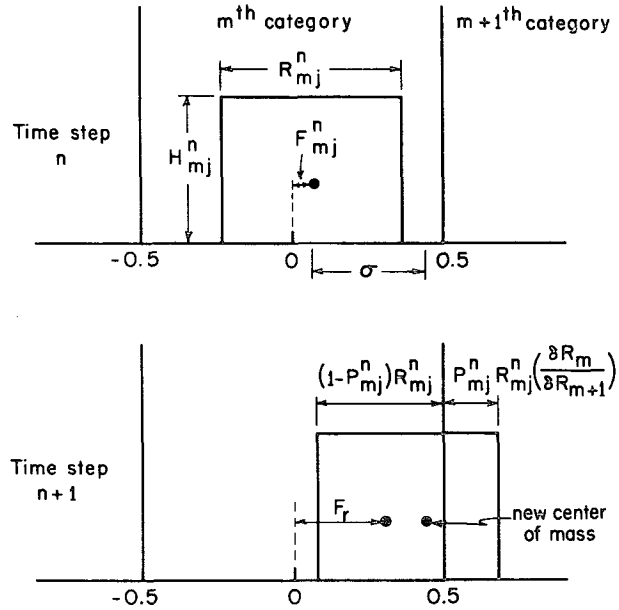

FIG. 16. Transfer of hydrometeor water between categories. Abscissa is R_m, radius of hydrometeors in category m. Ordinate is H_m, where $H_m dR_m$ is the mass of precipitation contained in particles with radii in the interval dR_m.

category and the changes in center of mass and spread caused by advection from different grid points, the following sequence of computation is adopted:

1) A tentative center of mass F^*_{mj} and spread R^*_{mj} is computed based only on the microphysical processes. Thus

$$(\rho_0 q_r)^*_{mj} F^*_{mj} = (\rho_0 q_r)_r F_r + (\rho_0 q_r)_a F_a + Q F^n_{mj},$$
$$(\rho_0 q_r)^*_{mj} R^*_{mj} = (\rho_0 q_r)_r [R_r^2 + 12(F^*_{mj} - F_r)^2] + (\rho_0 q_r)_a [R_a^2 + 12(F^*_{mj} - F_a)^2] + Q[R^{n2}_{mj} + 12(F^*_{mj} - F^n_{mj})^2],$$

where subscripts r and a denote quantities remaining and newly transferred, respectively, by the process described above. These two terms represent the average change in radius of the hydrometeors in any category due to the microphysical processes but they do not include the change in mass; Q represents the mass of water added or subtracted as a result of all the microphysical processes during a time step. The total mass in the mth category after the microphysical changes but before advection is

$$(\rho_0 q_r)^*_{mj} = (\rho_0 q_r)_r + (\rho_0 q_r)_a + Q.$$

2) Changes in the center of mass and spread by advection are then made:

$$(\rho_0 q_r)^{n+1}_{mj} F^{n+1}_{mj} = [(\rho_0 q_r)^*_{mj} - T^n_{mj}] F^*_{mj} + \sum_l I^n_{ml} F^*_{ml}$$

$$(\rho_0 q_r)^{n+1}_{mj} (R^{n+1}_{mj})^2 = [(\rho_0 q_r)^*_{mj} - T^n_{mj}] \times [R^{*2}_{mj} + 12(F^*_{mj} - F^{n+1}_{mj})^2] + \sum_l I^n_{ml} [R^{*2}_{ml} + 12(F^*_{ml} - F^{n+1}_{mj})^2],$$

where T^n_{mj} is the water transferred out of grid joint j and I^n_{ml} is the transfer into grid point j from grid point l. The total water in the mth category is now given by

$$(\rho_0 q_r)^{n+1}_{mj} = (\rho_0 q_r)^*_{mj} - T^n_{mj} + \sum_l I^n_{ml}.$$

REFERENCES

Asai, T., 1965: A numerical study of the air-mass transformation over the Japan Sea in winter. *J. Meteor. Soc. Japan*, **43**, 1–15.

Berry, E. X, 1967: Cloud droplet growth by collection. *J. Atmos. Sci.*, **24**, 688–701.

——, 1968: Modification of the warm rain process. Preprints *First Nat. Conf. Weather Modification*, Albany, Amer. Meteor. Soc., 81–85.

——, and R. L. Reinhardt, 1974a: An analysis of cloud drop growth by collection: Part I. Double distributions. *J. Atmos. Sci.*, **31**, 1814–1824.

——, and ——, 1974b: An analysis of cloud drop growth by collection: Part III. Accretion and self-collection. *J. Atmos. Sci.*, **31**, 2118–2126.

——, and ——, 1974c: An analysis of cloud drop growth by collection: Part IV. A new parameterization. *J. Atmos. Sci.*, **31**, 2127–2135.

Best, A. C., 1950: Empirical formulae for the terminal velocity of water drops falling through the atmosphere. *Quart. J. Roy. Meteor. Soc.*, **76**, 302–311.

Bigg, E. K., 1953: The formation of atmospheric ice crystals by the freezing of droplets. *Quart. J. Roy. Meteor. Soc.*, **79**, 510–519.

Braham, R. R., Jr., L. J. Battan and H. R. Byers, 1957: Artificial nucleation of cumulus clouds. *Meteor. Monogr.*, No. 11, Amer. Meteor. Soc., 47–85.

Brazier-Smith, P. R., S. G. Jennings and J. Latham, 1972: The interaction of falling water drops: coalescence. *Proc. Roy. Soc. London*, **A326**, 393–408.

——, —— and ——, 1973: Raindrop interactions and rainfall rates within clouds. *Quart. J. Roy. Meteor. Soc.*, **99**, 260–272.

Clark, T. L., 1973: Numerical modeling of the dynamics and microphysics of warm cumulus convection. *J. Atmos. Sci.*, **30**, 857–878.

Cooper, W. A., 1975: Reply to Fukuta (1975). *J. Atmos. Sci.*, **32**, 2371–2373.

Cotton, W. R., 1972: Numerical simulation of precipitation development in supercooled cumuli, Part 2. *Mon. Wea. Rev.*, **100**, 764–784.

Danielsen, E. F., R. Bleck and D. A. Morris, 1972: Hail growth by stochastic collection in a cumulus model. *J. Atmos. Sci.*, **29**, 135–155.

Egan, B. A., and J. R. Mahoney, 1972: Numerical modeling of advection and diffusion of urban area-source pollutants. *J. Appl. Meteor.*, **11**, 312–322.

English, M., 1973: Growth of large hail in the storm. Part II of *Alberta Hailstones*, *Meteor. Monogr.*, No. 36, Amer. Meteor. Soc., 37–98.

Fitzgerald, J. W., 1973: Dependence of the supersaturation spectrum of CCN on aerosol size distribution and composition. *J. Atmos. Sci.*, **32**, 628–634.

Fukuta, N., 1975: Comments on "A possible mechanism for contact nucleation." *J. Atmos. Sci.*, **32**, 2371–2373.

Heymsfield, A. J., 1978: The characteristics of graupel particles in northeastern Colorado cumulus congestus clouds. *J. Atmos. Sci.*, **35**, 284–295.

Kessler, E., 1969: On the distribution and continuity of water substance in atmospheric circulation. *Meteor. Monogr.*, No. 32, Amer. Meteor. Soc., 84 pp.

Komabayasi, M., T. Gonda and K. Isono, 1964: Life-time of water drops before breaking and size distribution of fragment droplets. *J. Meteor. Soc. Japan*, **19**, 236–243.

Leighton, H. G., and R. R. Rogers, 1974: Droplet growth by condensation and coalescence in a strong updraft. *J. Atmos. Sci.*, **31**, 271–279.

List, R., and J. R. Gillespie, 1976: Evolution of raindrop spectra with collision-induced breakup. *J. Atmos. Sci.*, **33**, 2007–2013.

Macklin, W. C., 1963: Heat transfer by hailstones. *Quart. J. Roy. Meteor. Soc.*, **89**, 360–369.

——, and I. H. Bailey, 1968: The collection efficiencies of hailstones. *Quart. J. Roy. Meteor. Soc.*, **94**, 393–396.

Marshall, J. S., and W. M. K. Palmer, 1948: The distribution of raindrops with size. *J. Meteor.*, **5**, 165–166.

Mason, B. J., 1971: *The Physics of Clouds*. Clarendon Press, 671 pp.

——, and J. B. Andrews, 1960: Dropsize distribution from various types of rains. *Quart. J. Roy. Meteor. Soc.*, **86**, 301–314.

McTaggart-Cowan, J. D., and R. List, 1975: Collision and breakup of water drops at terminal velocity. *J. Atmos. Sci.*, **32**, 1401–1411.

Nakaya, U., 1954: *Snow Crystals*. Harvard University Press, 510 pp.

Nelson, L. D., 1971: A numerical study on the initiation of warm rain. *J. Atmos. Sci.*, **28**, 752–762.

Saunders, P. M., 1965: Some characteristics of tropical marine showers. *J. Atmos. Sci.*, **22**, 167–175.

Scott, B. C., and P. V. Hobbs, 1977: A theoretical study of the evolution of mixed-phase cumulus clouds. *J. Atmos. Sci.*, **34**, 812–826.

Silverman, B. A., and M. Glass, 1973: A numerical simulation of warm cumulus clouds: I. Parameterized vs. non-parameterized microphysics. *J. Atmos. Sci.*, **30**, 1620–1637.

Spengler, J. D., and N. R. Gokhale, 1973: Drop impaction. *J. Appl. Meteor.*, **12**, 316–321.

Srivastava, R. C., 1971: Size distribution of raindrops generated by their breakup and coalescence. *J. Atmos. Sci.*, **28**, 410–415.

Vali, G., 1968: Ice nuclei relevant to formation of hail. Sci. Rep. MW-58, Stormy Weather Group, McGill University, Canada, 51 pp.

Whelpdale, D. M., and R. List, 1971: The coalescence process in raindrop growth. *J. Geophys. Res.*, **76**, 2836–2856.

Yau, M.-K., 1973: A kinematic model to study the distribution of precipitation in a cumulus updraft. S.M. thesis, Department of Meteorology, MIT, 91 pp.

Young, K. C., 1974a: The role of contact nucleation in ice phase initiation in clouds. *J. Atmos. Sci.*, **31**, 768–776.

——, 1974b: A numerical simulation of wintertime, orographic precipitation. I, description of model microphysics and numerical technique. *J. Atmos. Sci.*, **31**, 1735–1748.

——, 1975: The evolution of drop spectra due to condensation, coalescence and breakup. *J. Atmos. Sci.*, **32**, 965–973.